Efficient HRTF Computation using Adaptive Rectangular Decomposition

Alok Meshram[1], Ravish Mehra[1], and Dinesh Manocha[1]

[1]*Dept. of Computer Science, University of North Carolina at Chapel Hill, 201 South Columbia Street, NC, 27599-3175 USA*
http://gamma.cs.unc.edu/HRTF/

Correspondence should be addressed to Alok Meshram (alok@cs.unc.edu)

ABSTRACT

Accurate rendering of spatial audio over headphones requires the use of personalized head related transfer functions (HRTFs). These HRTFs are difficult to obtain due to the tedious and expensive measurement process requiring an anechoic chamber. An alternate approach uses accurate 3D meshes of human head and torso and numerical simulation techniques to compute personalized HRTFs. While these simulation techniques can compute accurate HRTFs, they require hours or days of computation on a desktop machine. We present an efficient technique to compute personalized HRTFs, combining a fast numerical solver, called adaptive rectangular decomposition, with the acoustic reciprocity principle and the Kirchhoff surface integral representation to reduce the overall computation. This technique requires only two numerical simulations and can compute the HRTF in 20 minutes on a desktop machine. We highlight the performance of our technique on the Fritz and KEMAR benchmarks and compare with measurements to test its accuracy.

1. INTRODUCTION

The human auditory system's ability to localize the direction of incoming sound based on the sound signals received at the ears is attributed to cues such as interaural time difference, interaural intensity difference and spectral modification due to the scattering of sound waves due to the body [4]. 3-D sound systems often incorporate these cues into the audio rendering, which is usually accomplished through the use of head related transfer functions (HRTFs) [18, 3].

A significant challenge involving the use of HRTFs is the variation of head, pinna and torso geometries, and the corresponding variation in HRTFs across individuals. The HRTF measurement techniques that have been traditionally used to obtain personalized HRTFs often require the use of specialized, expensive equipment as well as tedious processes where subjects must sit still for long periods of time [2, 21]. As a result, personalized HRTFs of individuals are very rarely available and virtual auditory displays usually resort to using generic HRTFs [20]. The use of such non-personalized HRTFs can lead to problems: lack of externalization, front-back confusions and reversals, incorrect elevation perception, and overall unconvincing spatializations [4, 3, 17]. This has motivated the need to develop efficient techniques to obtain personalized HRTFs for individuals.

One approach to solving this problem is based on the idea that HRTF measurement can be considered to be an acoustic scattering problem in free-field [5]. Given the 3D mesh of a human body and its acoustic properties, numerical sound simulation techniques can be used to compute HRTFs. Techniques such as the boundary element method [8, 5] and the finite-difference time-domain method [19, 10, 11] have been used to compute HRTFs. The accuracy of these computed HRTFs has been demonstrated by comparing them with measurements. However, these techniques are computationally expensive, taking tens of hours or even days on desktop machines.

Main results We present an efficient technique for computing personalized HRTFs using a state-of-the-art numerical simulation technique called *adaptive rectangular decomposition* (ARD). To reduce computation time, we make use of the acoustic reciprocity principle to reduce number of simulations required and the Kirchhoff surface integral representation (KSIR) to reduce the size of the simulation domain. Our technique requires only 20 minutes of simulation time to compute broadband HRTFs on a 8-core desktop machine compared to hours

or days taken by other techniques. We analyze the accuracy of our approach by using it to compute the left-ear HRTF of the Fritz and KEMAR manikins. The mean spectral mismatch between the HRTF computed by our technique and measurements was 3.88 dB for Fritz and 3.58 dB for KEMAR, within a linear frequency range from 700 Hz to 14 kHz. Qualitatively, we observe a good match between the computed and measured HRTFs for both manikins.

2. PRIOR WORK

Measurement

The most common method for obtaining personalized HRTFs is acoustic measurements. Measurements are usually done in an anechoic chamber with an array of high-quality speakers arranged in a spherical pattern. The subject is made to sit at the center of this sphere. A high-quality probe microphone is inserted into the ears of the subject, usually at the entrance of blocked ear canals or inside open ear canals. The subject is instructed to sit still for the duration of the measurements. A specific signal (such as Golay-coded signals) is played one by one from the different speakers, and the signals at the microphones are recorded and stored. These recordings are then post-processed to generate the HRTFs. In the past decade, various techniques have been proposed by researchers to perform these measurements [2, 21, 12]; however, since such measurements usually require expensive equipment along with tedious procedures, they are conducted mainly for research purposes, and their widespread use is limited.

Numerical Simulation

Many numerical simulation techniques have been used to compute HRTFs. These techniques take the 3D mesh of the human head and torso as input and solve the acoustic wave equation to model scattering of sound. Two commonly used techniques are the boundary element method (BEM) [8, 6] and the finite-difference time-domain (FDTD) method [19, 10, 11]. Gumerov et al. [5] reported HRTF computation for the KEMAR manikin using parallelized fast multipole method accelerated BEM. While they presented qualitative visual comparison of the computed HRTFs with measurements, quantitative comparisons between measured and computed data were not presented. Also, the simulation time was in tens of hours on a desktop machine. Mokhtari et al. [11, 10] reported HRTF computation for the KEMAR manikin and human subjects using a combination of FDTD and Kirchhoff-Helmholtz integral equation. Quantitative comparison between computed HRTFs and measured HRTFs were presented, but the simulation time was not reported for these computations. A comparison of the prior simulation techniques is provided in Table 1.

3. HRTF COMPUTATION PIPELINE

A broad overview of our HRTF computation pipeline is presented in Figure 1. We assume that a closed, accurate 3-D mesh of the head and torso of the subject is available. The 3-D mesh of the head and torso is placed at the center of an empty cuboidal simulation domain. We construct an offset surface around the head to serve as the KSIR surface. The size of this domain is chosen such that it closely fits the head and torso mesh, as well as a cuboidal KSIR surface surrounding the head. A point close to each of the blocked ear canal entrances is manually picked as receiver position for the HRTF computation. The source positions are uniformly chosen at a fixed distance (usually 1m) away from the center of the head at different orientations.

Two ARD simulations (one for each ear) are then run using this simulation domain. The principle of acoustic reciprocity[1] is used to reverse the role of source and receivers: The aforementioned receiver positions are used as source positions for these simulations, and the original source positions as receiver positions. The simulation domain is surrounded by perfectly absorbing layer to prevent reflections from domain boundaries.

These simulations produce pressure signals at each grid cell within the simulation domain, including the KSIR surface. The pressure signals at the KSIR surface are used as input by the Kirchhoff surface integral formulation, generating pressure signals at the reciprocal receiver positions. These signals are the pressure responses at the ear positions due to the original sources around the head. These are then used to compute HRTFs using the following equations:

$$H_L(\theta,\phi,\omega) = \frac{X_L(\theta,\phi,\omega)}{X_C(\theta,\phi,\omega)} \tag{1}$$

$$H_R(\theta,\phi,\omega) = \frac{X_R(\theta,\phi,\omega)}{X_C(\theta,\phi,\omega)}, \tag{2}$$

where $X_L(\theta,\phi,\omega)$ and $X_R(\theta,\phi,\omega)$ are the Fourier transforms of the left-ear and right-ear time-domain pressure

[1] The principle of acoustic reciprocity states that we can reverse the sense of source and listener without changing the acoustic response [13, p. 195-199]

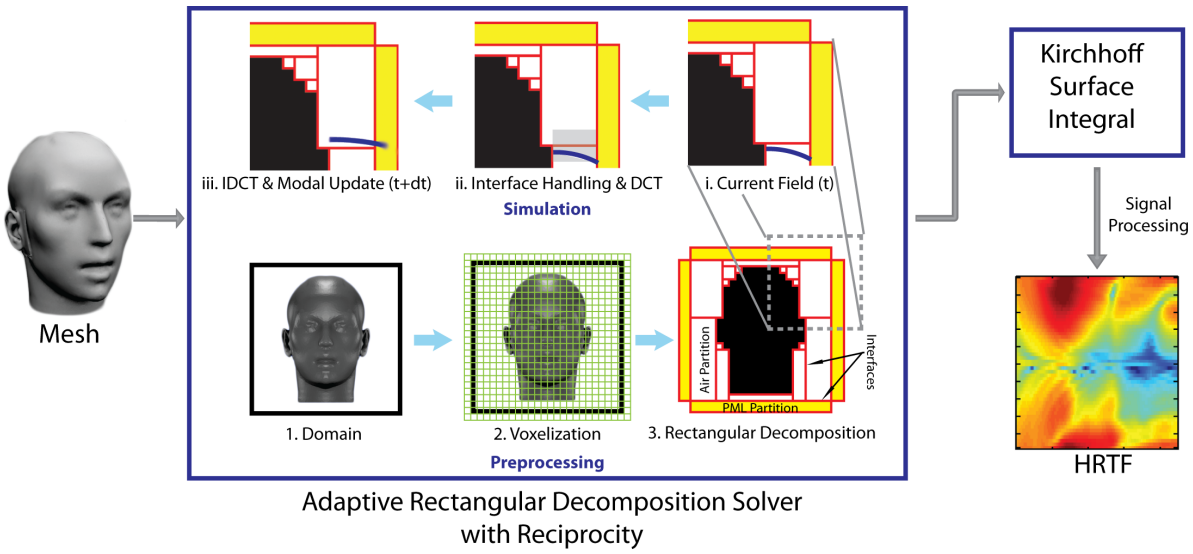

Fig. 1: An overview of our HRTF computation pipeline showing details of the different stages of the adaptive rectangular decomposition (ARD) solver. We start with a 3D mesh of the human head and perform ARD simulations while exploiting the acoustic reciprocity principle, generating a sound field on an offset surface around the head. We then apply the Kirchhoff surface integral on the resulting sound fields to compute the HRTF corresponding to each ear.

signals for the original source at azimuth θ and elevation ϕ, and $X_C(\theta,\phi,\omega)$ is the Fourier transform of the signal received at the origin due to the same source in the absence of the listener, all in free-field conditions.

4. COMPUTATIONAL METHODS

In this section, we present the details of each stage of our HRTF computation pipeline.

4.1. Adaptive Rectangular Decomposition

Our pipeline uses Adaptive Rectangular Decomposition (ARD) for sound propagation simulation [14, 9]. Like finite-difference-based methods, ARD divides the simulation domain into grid cells and computes sound pressure at each of those grid cells at each time step. However, compared to finite-difference-based methods, ARD has much lower numerical dispersion error while being at least an order of magnitude faster. The principle behind ARD's efficiency and accuracy is its use of the exact analytical solution of the wave equation within cuboidal domains consisting of a homogeneous, dissipation-free medium:

$$p(x,y,z,t) = \sum_{i=(i_x,i_y,i_z)} m_i(t)\cos\left(\frac{\pi i_x}{l_x}x\right)\cos\left(\frac{\pi i_y}{l_y}y\right)\cos\left(\frac{\pi i_z}{l_z}z\right), \quad (3)$$

where $p(x,y,z,t)$ is the pressure field (or sound signal) at position (x,y,z) and at time t, (l_x,l_y,l_z) are the extents of the cuboidal region, and $m_i(t)$ are time-varying mode coefficients. As this solution is composed of cosines, ARD uses efficient Fast Fourier Transform techniques to compute propagation within the cuboidal region.

Figure 1 shows the different stages of the ARD simulator as part of our pipeline. In the preprocessing stage (bottom row of the ARD block in Figure 1), the domain is first voxelized. This generates a grid of voxels that are then grouped together to form cuboidal regions called air partitions. Boundary conditions are applied by using perfectly matched layer (PML) partitions at the boundary to simulate both partially- and completely-absorbing surfaces.The simulation stage (top row of the ARD block in Figure 1) consists of two updates: interface handling and pressure update. The interface handling step uses finite-difference stencils to propagate sound across adjacent partitions. In the pressure update step, the time varying mode coefficients for each air partition are updated based on the acoustic wave equation to propagate sound within partitions.

4.2. Acoustic Reciprocity

HRTFs are functions of source positions and are measured for multiple source positions. Exact replication of this process through numerical simulation requires mul-

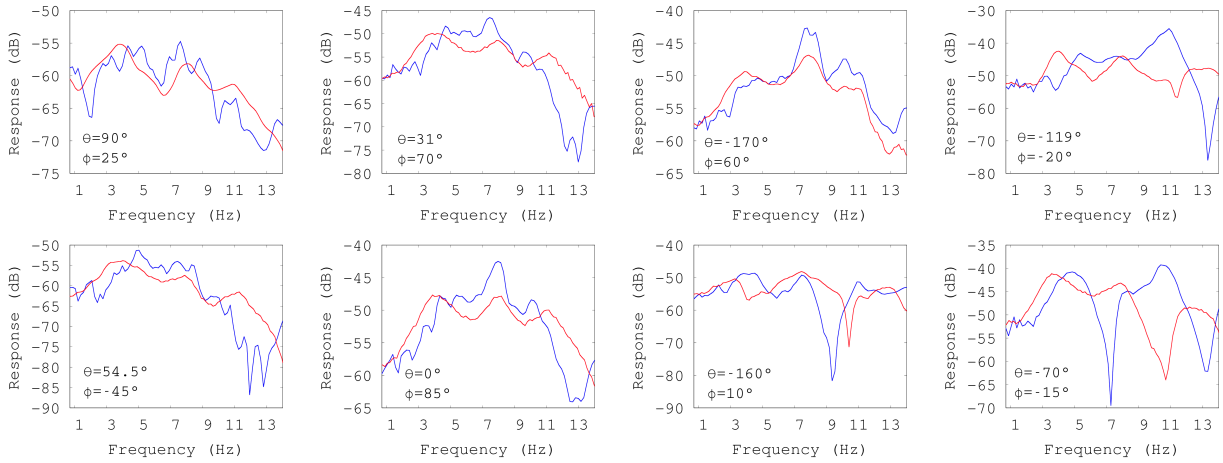

Fig. 2: Comparison of measured (blue) and computed (red) HRTFs of Fritz for 8 non-horizontal plane source positions. Source position is specified in a vertical polar coordinate system used by the measurement dataset. Azimuth θ is in the interval $[-180, 180]$ degrees, 0 degree azimuth in the front, and positive azimuth to the right of the listener. Elevation ϕ is in $[-90, 90]$ degrees, with 0 degree elevation in the horizontal plane, and positive elevation to the top of the listener.

tiple simulations, one for each source position. This results in prohibitively high computation time for computing the full HRTF of an individual. Our technique avoids this cost by utilizing the principle of acoustic reciprocity. This principle states that we can reverse the sense of source and listener without changing the acoustic response [13, p. 195-199]. This allows us to obtain a full HRTF by placing the source at the receiver position inside the ear. This reduces the required number of simulations to just two, one for each ear.

4.3. Kirchhoff Surface Integral Representation

HRTFs are measured at a fixed distance from the center of the head of the subject. Therefore, In order to compute the full HRTF as described above, a simulation domain with a radius equal to this distance is required. This distance is usually around 1.0 m, due to which the simulation domain is mostly empty as the size of the head and torso is relatively small. Since computation time required by ARD scales cubically with simulation domain dimension, this can lead to large computation times. To reduce the size of the simulation domain, we make use of the Kirchhoff surface integral representation (KSIR) [15]. This representation enables the computation of pressure values outside the simulation domain by using pressure values at a tight-fitting surface that encloses the head and torso, resulting in a significantly smaller simulation domain and faster simulations.

5. EVALUATION

In order to evaluate our technique, we used it to generate left-ear HRTFs for KEMAR with DB-60 pinnae and the Fritz manikin using their scanned 3D models. In this section, we present both quantitative and qualitative comparison of the measured HRTFs of these manikins with those computed by our pipeline. Before presenting these results, we discuss pertinent simulation parameters.

5.1. Simulation Parameters

The speed of sound within the homogeneous, dissipation-free medium of ARD simulation was set to 343 ms^{-1} to match that of air. Second-order finite-difference stencils were used in ARD for interface handling. To have a small grid cell size of 1.94 mm, the maximum simulation frequency for ARD was set to 88.2 kHz. A Gaussian impulse source with a center frequency of 33.075 kHz was used as source signal. The absorption coefficient of the mesh surface was set to 0.02 to correspond to that of human skin, as reported in Ackerman et. al. [1]. The simulations were run to generate 5.0 ms pressure signals.

5.2. Comparison with Measured HRTFs

To quantitatively compare the computed and measured HRTF datasets, we make use of a mean spectral distance

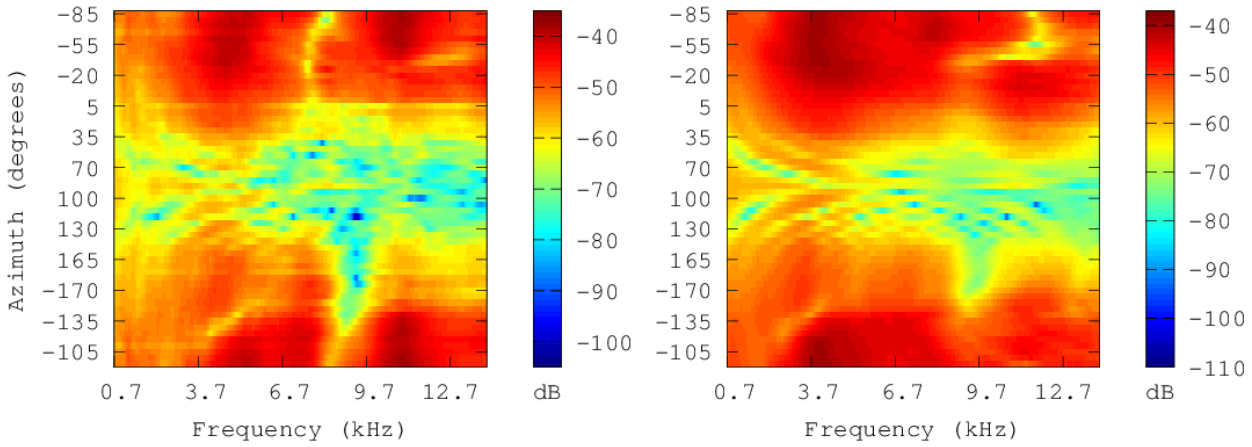

Fig. 3: Comparison of measured (left) and computed (right) HRTFs of Fritz at 58 azimuth angles in the horizontal plane. Azimuth angles range from -180 degrees to 180 degrees, with 0 degree azimuth corresponding to the source at the front of the head.

(MSD) measure, defined as:

$$MSD = \frac{1}{M}\sum_{i=1}^{M}\frac{\|H^i_{L,m}(\omega) - H^i_{L,s}(\omega)\|_1}{N}, \qquad (4)$$

where M refers to the number of source positions for which HRTF measurement are available, N refers to the number of frequencies for which the comparison is made, i refers to the ith source position, and $H^i_{L,m}(\omega)$ and $H^i_{L,s}(\omega)$ are vectors of length N that represent the log-magnitude spectra of the measured and computed left-ear HRTFs respectively, specified in dB.

The values of the parameters M and N depend on the measurement dataset. While M is the number of source positions for which the HRTFs were measured in the dataset, the value of N depends on the frequency range within which comparison is made. In general, HRTF measurement data is considered unreliable below 700 Hz and above 14 kHz [5]. As a result, we compare computed and measured HRTFs in the 700 Hz to 14 kHz range.

To analyze the simulator's accuracy in computing the HRTFs, we ran these simulations without KSIR using a domain of dimensions 2.8 m $\times$2.8 m $\times$2.8 m so that pressure values 1.0 m away from the head can be obtained directly through the ARD simulation.

Fritz

The scanned 3-D mesh of the Fritz manikin was obtained from Dr. Ramani Duraiswami [5]. The mesh consisted of the head only, and did not have a torso. Measured HRTF data for Fritz was obtained from the measurements that were part of the "Club Fritz" activity [7]. In this dataset, measurements are provided for 823 source positions.

Quantitatively, we observe an MSD error of 3.58 dB between the measured HRTFs and those computed by our technique. This is comparable to the MSD value of 3.1 dB between the measured left and right ear HRTFs of KEMAR at equivalent source positions [11].

Figure 3 presents a comparison between the measured and computed HRTFs within the horizontal plane. The figure shows a broad match between the shapes of the HRTFs as well as matching detailed features, such as the finger-like projections at low frequencies between the azimuth range of 5 to 165 degrees, the trough between 8-10 kHz at the azimuths within the 130 to 180 degree range, and the peak between 4-6 kHz in the azimuths between -20 to -135 degrees. Some mismatch, especially for the azimuths close to the left ear, can also be observed.

Figure 2 presents a comparison between the computed and measured HRTFs for eight source positions at varying azimuths and elevations not in the horizontal plane. These graphs show an overall match between the features of the HRTFs in terms of peaks and notches, especially below 10 kHz. The biggest mismatch can be observed for the HRTFs in the right-most column, which correspond to source positions below the listener. This mismatch is observed for all source positions below the listener, and may come from the lack of torso in our simulations.

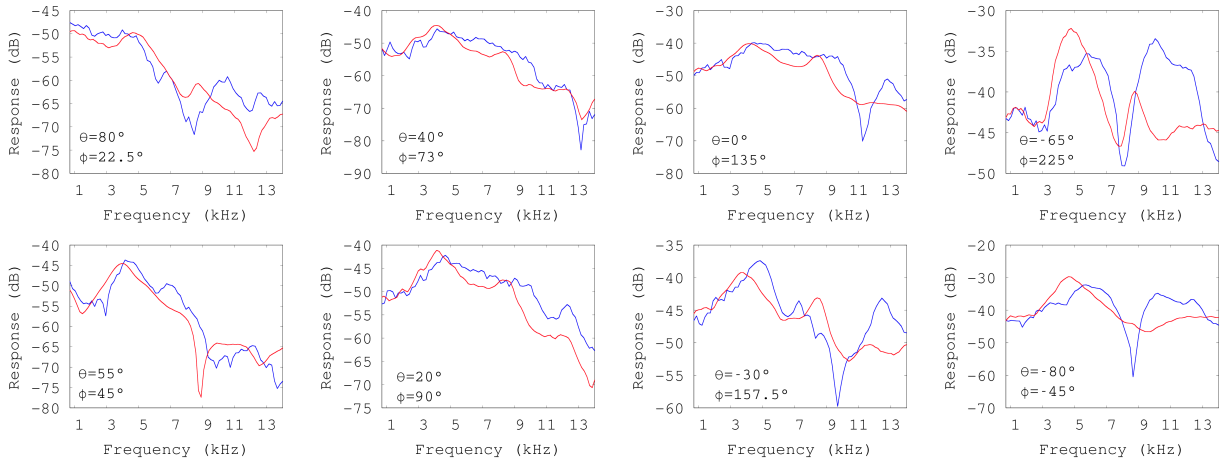

Fig. 4: Comparison of measured (blue) and computed (red) HRTFs of KEMAR for 8 non-horizontal plane source positions. Source position is specified in an interaural polar coordinate system used by the measurement dataset. Azimuth θ is in the interval $[-90, 90]$ degrees, 0 degree azimuth in the front, and positive azimuth to the right of the listener. Elevation ϕ is in $[-90, 270]$ degrees, with 0 degree elevation in the horizontal plane, and positive elevation to the top of the listener.

KEMAR with DB-60 Pinnae

The scanned 3-D meshes of the KEMAR manikin and of the DB-60 pinna were obtained from Dr. Yuvi Kahana [6]. Since these meshes were separate, we manually stitched the mesh of DB-60 pinna into the KEMAR mesh. Again, the torso mesh was not available, so we ran our simulations only on the head mesh. Measured HRTF data for the KEMAR manikin was obtained from the CIPIC HRTF database [2], where subject 165 is KEMAR with DB-60 pinnae. In this database, HRTF measurements are provided for 1250 source positions.

We observe an MSD error of 3.58 dB between the computed and measured HRTFs for KEMAR. Again, this is comparable to the MSD value of 3.1 dB between equivalent left and right ear measured HRTFs of KEMAR.

Figure 5 presents a qualitative comparison between the measured and computed HRTFs. Once again, an overall match between the shapes of the HRTFs can be observed; matching features include the finger-like features in the low frequencies between 40 and 145 degrees azimuth and the peak within the $4-7$ kHz range for the -10 to -80 degrees azimuths. For KEMAR, we observe greater mismatch between the computed and measured HRTFs in the horizontal plane, especially for frequencies above 7 kHz. This could be due to the manual stitching procedure we used to join the pinna and head mesh.

For non-horizontal source positions, Figure 4 compares the computed and measured HRTFs for eight source positions at varying azimuths and elevations. As with Fritz, a good overall match is observed in terms of features such as peaks and notches. Also like Fritz, some features such as notches are sometimes missing above 10 kHz, and there is a broad mismatch for elevations below the listener (rightmost column), which could be due to the absence of the torso mesh in our simulations.

5.3. Comparison with previous techniques

Table 1 provides a comparison of our technique with previous HRTF computation techniques, also providing the computation time required by our technique. Katz et al. [8] used BEM to compute the HRTF of a human subject, requiring multiple simulations at different frequencies to compute a full HRTF. They computed HRTF for different directions by running separate simulations for each direction. Gumerov et al. [5] used a fast multipole method accelerated BEM (FMMBEM), which has lower computational cost than conventional BEM. They used the reciprocity principle to reduce the number of simulations required for computation of HRTF for different directions. However, this technique also requires multiple simulations at different frequencies. The authors computed the HRTFs of KEMAR and Fritz and compared with measurements, showing reasonably high accuracy.

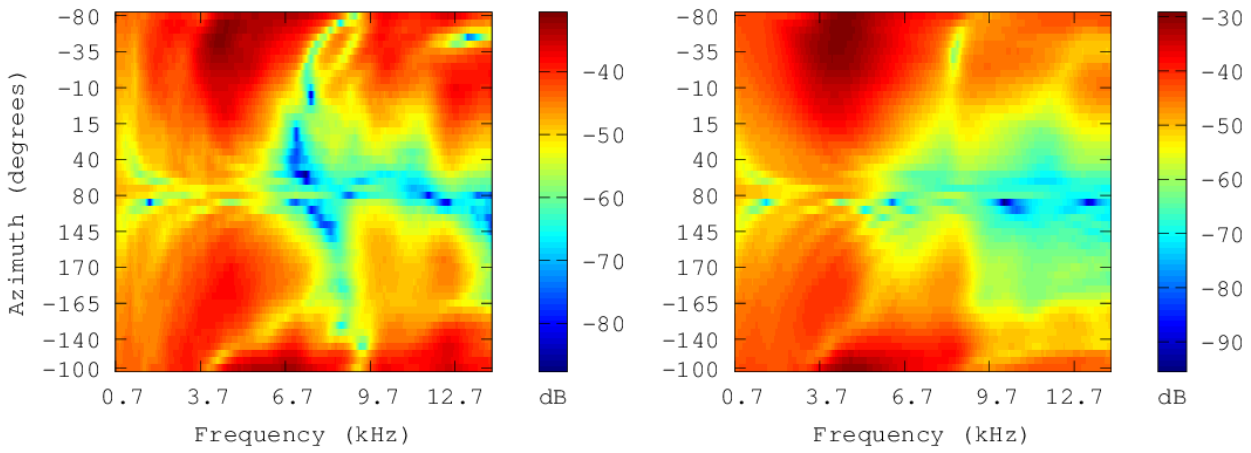

Fig. 5: Comparison of measured (left) and computed (right) HRTFs of KEMAR with DB-60 pinnae at 50 azimuth angles in the horizontal plane and at 50 elevation angles in the median plane (bottom).

Compared to BEM which usually requires multiple simulations at different frequencies to compute a full HRTF, FDTD is a time-domain technique that can compute the HRTF in a wide frequency range in a single simulation. Also, FDTD is a grid-based solver, which avoids the mesh discretization step in BEM. Xiao et al. [19] used a FDTD solver to compute the HRTF of KEMAR. To reduce computation cost, they used the scattered field/total field formulation. However, they ran different simulations for each direction the HRTF was computed in. Mokhtari et al. [11] used FDTD with the Kirchhoff-Helmholtz integral equation to reduce the simulation domain size, resulting in lower computation cost. They also used the reciprocity principle. They provided qualitative as well as quantitative comparison of KEMAR's computed and measured HRTFs, reporting a mean spectral distance of 2.3 dB for the right ear HRTF.

Our pipeline uses ARD combined with Kirchoff surface integral representation and the reciprocity principle. ARD is a grid-based solver like FDTD. Also like FDTD, it computes an HRTF in a wide frequency range in a single simulation. However, ARD is at least an order of magnitude faster than FDTD, resulting in overall lower computational cost compared to FDTD.

6. CONCLUSION AND FUTURE WORK

We presented an HRTF computation technique that is based on adaptive rectangular decomposition, and have demonstrated computed HRTFs of the Fritz and KEMAR manikins. Qualitatively, we observe a broad match with measurements while also observing some mismatching or absent detailed features, especially at high frequencies. Quantitatively, we observed an MSD error of 3.88 dB for Fritz and 3.58 dB for KEMAR.

Various factors could be contributing to these errors. An important source of error is the absence of the torso mesh in our computations. Inaccuracies in the head meshes, and the exact placement and orientation of the mesh with respect to the source positions, may differ from that in the measurements; this may be another source of error. This is especially probable for KEMAR, since the manual stitching process could have resulted in an erroneous position of the pinna. Finally, some limitations of ARD might also contribute to error. ARD uses frequency independent absorption coefficients while measurements indicate variation of absorption coefficients with frequency. Another limitation is ARD's inability to simulate transmission of sound waves through objects.

While the HRTFs computed by our pipeline have some qualitative mismatch with measurements and higher MSD error compared to state-of-the-art FDTD based techniques [11], our pipeline computes HRTFs within 20 minutes on a desktop machine compared to hours or days taken by other techniques. This can contribute towards attaining the goal of practical use of personalized HRTFs in virtual auditory displays.

Future work involves using our technique to compute HRTFs for human subjects and investigating their lo-

Technique	Subject	Simulation Method	Maximum Frequency	Computation Time	Computation Platform	Measurement Comparison
Katz et al. [8]	Human subject	BEM	5.4 kHz	28 hrs/freq.	-	-
Xiao et al. [19]	KEMAR	FDTD	7.0 kHz	0.66 hrs/dir.	SUN Ultra 60	-
Mokhtari et al. [11]	KEMAR	FDTD	22.0 kHz	-	-	Qualitative & Quantitative
Gumerov et al. [5]	KEMAR, Fritz	FMMBEM	20.155 kHz	KEMAR: 14 hrs, Fritz: 32 hrs	4 core CPU at 2.66 GHz	Qualitative
Tang et al. [16]	BHead210	BEM	10.0 kHz	-	-	Qualitative
Our method	KEMAR, Fritz	ARD	22.0 kHz	KEMAR, Fritz: 20 mins	8 core CPU at 3.40 GHz	Qualitative & Quantitative

Table 1: Comparison of our technique with previous techniques using numerical simulation to compute HRTFs.

calization performance with the computed HRTFs compared to measured and generic HRTFs.

7. ACKNOWLEDGMENTS

We would like to thank Dr. Yuvi Kahana and Institute for Sound and Vibration Research (ISVR), University of Southampton, UK, for the scanned 3-D mesh of the KEMAR manikin and DB-60 pinna as well as Dr. Ramani Duraiswami and Dr. Dmitry Zotkin at University of Maryland, USA, for the scanned 3-D mesh and HRTFs of the Fritz manikin.

This research was supported by Link Foundation Fellowship in Advanced Simulation and Training, ARO Contracts W911NF-10-1-0506, W911NF-12-1-0430, W911NF-13-C-0037, and the National Science Foundation (NSF awards 0917040, 1320644).

8. REFERENCES

[1] E. Ackerman and F. Oda. Acoustic absorption coefficients of human body surfaces. Technical report, DTIC Document, 1962.

[2] V. R. Algazi, R. O. Duda, D. M. Thompson, and C. Avendano. The cipic hrtf database. In *Applications of Signal Processing to Audio and Acoustics, 2001 IEEE Workshop on the*, pages 99–102. IEEE, 2001.

[3] D. R. Begault. *3-D Sound for Virtual Reality and Multimedia*. Academic Press, 2000.

[4] J. Blauert. *Spatial hearing: the psychophysics of human sound localization*. MIT press, 1997.

[5] N. A. Gumerov, A. E. ODonovan, R. Duraiswami, and D. N. Zotkin. Computation of the head-related transfer function via the fast multipole accelerated boundary element method and its spherical harmonic representation. *The Journal of the Acoustical Society of America*, 127:370, 2010.

[6] Y. Kahana and P. A. Nelson. Boundary element simulations of the transfer function of human heads and baffled pinnae using accurate geometric models. *Journal of sound and vibration*, 300(3):552–579, 2007.

[7] B. Katz and D. R. Begault. Round robin comparison of hrtf measurement systems: preliminary results. In *Proc. 19th Intl. Congress on Acoustics (ICA2007), Madrid, Spain*, 2007.

[8] B. F. Katz. Boundary element method calculation of individual head-related transfer function. i. rigid model calculation. *The Journal of the Acoustical Society of America*, 110:2440, 2001.

[9] R. Mehra, N. Raghuvanshi, M. Lin, and D. Manocha. Efficient GPU-based Solver for Acoustic Wave Equation. Technical report, Department of Computer Science, UNC Chapel Hill, USA, 2010.

[10] P. Mokhtari, H. Takemoto, R. Nishimura, and H. Kato. Computer simulation of hrtfs for personalization of 3d audio. In *Universal Communication, 2008. ISUC'08. Second International Symposium on*, pages 435–440. IEEE, 2008.

[11] P. Mokhtari, H. Takemoto, R. Nishimura, and H. Kato. Computer simulation of kemar's head-related transfer functions: verification with measurements and acoustic effects of modifying head shape and pinna concavity. *Principles and Applications of Spatial Hearing*, pages 179–194, 2010.

[12] M. Pec, M. Bujacz, and P. Strumiłło. Personalized head related transfer function measurement and verification through sound localization resolution. In *Proceedings of the 15th European Signal Processing Conference*, pages 2326–2330, 2007.

[13] A. D. Pierce. *Acoustics: An Introduction to Its Physical Principles and Applications*. Acoustical Society of America, 1989.

[14] N. Raghuvanshi, R. Narain, and M. C. Lin. Efficient and accurate sound propagation using adaptive rectangular decomposition. *Visualization and Computer Graphics, IEEE Transactions on*, 15(5):789–801, 2009.

[15] O. M. Ramahi. Near-and far-field calculations in fdtd simulations using kirchhoff surface integral representation. *Antennas and Propagation, IEEE Transactions on*, 45(5):753–759, 1997.

[16] L. Tang, Z.-H. Fu, and L. Xie. Numerical calculation of the head-related transfer functions with chinese dummy head. In *Signal and Information Processing Association Annual Summit and Conference (APSIPA), 2013 Asia-Pacific*, pages 1–4. IEEE, 2013.

[17] E. M. Wenzel, M. Arruda, D. J. Kistler, and F. L. Wightman. Localization using nonindividualized head-related transfer functions. *The Journal of the Acoustical Society of America*, 94:111, 1993.

[18] F. L. Wightman and D. J. Kistler. Headphone simulation of free-field listening. i: Stimulus synthesis. *The Journal of the Acoustical Society of America*, 85:858, 1989.

[19] T. Xiao and Q. H. Liu. Finite difference computation of head-related transfer function for human hearing. *The Journal of the Acoustical Society of America*, 113:2434, 2003.

[20] B. Xie. *Head-related transfer function and virtual auditory display*. Plantation, FL: J. Ross Publishing, 2013.

[21] B. Xie, X. Zhong, D. Rao, and Z. Liang. Head-related transfer function database and its analyses. *Science in China Series G: Physics, Mechanics and Astronomy*, 50(3):267–280, 2007.